RESEARCH ARTICLE

CrossMark

The influence of topographic roughness on lava flow emplacement

M. Elise Rumpf[1,2] • Einat Lev[1] • Robert Wysocki[3]

© This is a U.S. Government work and not under copyright protection in the US; foreign copyright protection may apply 2018

Abstract

A quantitative understanding of the factors controlling lava flow emplacement is critical for both hazard assessment and mitigation and for the interpretation of past flow emplacement conditions. The influence of topography with a vertical amplitude smaller than flow thickness (i.e., substrate roughness) is currently not accounted for in most flow emplacement models and hazard estimates. Here, we measure the effect of substrate roughness on flow emplacement through experiments using analog fluids and molten basalt, complementing recent work on the interaction of lava flows with obstacles taller than flow thickness. We present results from three sets of analog experiments, in which corn syrup, polyethylene glycol, and molten basalt were each extruded onto a sloping plane covered with a series of beds of varying grain sizes. We find that flow front advance rates are impacted by bed roughness for all materials, with decreases in average velocities by up to 50% with increases of substrate grain sizes by 5–100 times, ranges analogous with topographic variations found in nature. These decreases in flow front advance velocities are equivalent to up to an order of magnitude increase in fluid viscosity. We interpret this velocity decrease to be caused by the movement of material into void spaces between substrate grains and by enhanced cooling through heat conduction to the substrate due to increased surface contact area. The difference in advance velocity with increasing grain size diminishes with time after initial emplacement as a basal boundary layer is established. Additionally, the experimental flow geometry, measured by the complexity of the flow external perimeter, became increasingly complex with increasing substrate grain size. This effect will act to both slow the forward advance of lava flows and to create irregular emplacement paths of flows moving over rough surfaces. We propose that flow emplacement models should be modified, possibly through a calibrated "effective viscosity" term, to account for bed roughness to increase accuracy in flow prediction and hazard estimation models.

Keywords Lava viscosity · Lava dynamics and cooling · Experimental volcanology · Volcano hazards · Analog experiments

Introduction

The emplacement of basaltic lava is a complex process that depends on many factors, including the rheological properties

✉ M. Elise Rumpf
   mrumpf@usgs.gov

1 Lamont-Doherty Earth Observatory, Columbia University, 61 Route 9W, Palisades, NY 10964, USA

2 U.S. Geological Survey, Astrogeology Science Center, Flagstaff, AZ 86001, USA

3 School of Art, Syracuse University, Syracuse, NY 13244, USA

of the lava, the rate of lava effusion, and the environment into which they are emplaced (e.g., Walker 1973; Rowland and Walker 1990; Griffiths 2000; Harris and Rowland 2009). Our ability to predict this behavior relies on a clear understanding of the physical mechanisms that control lava–environment interactions. Previous studies have addressed the influence of a multitude of factors on flow emplacement, including gravity, ground slope and slope changes, lava composition, and atmospheric conditions such as ambient temperature, atmospheric pressure, and precipitation (e.g., Pinkerton and Wilson 1994; Keszthelyi and Self 1998, Glaze et al. 2014). Numerical models have shown that physical properties of the substrate beneath a lava flow, such as composition, porosity, and cohesion, can also affect flow dynamics and cooling (e.g., Fagents and Greeley 2001; Fagents et al. 2010; Rumpf et al. 2013a). The influence of topography on lava flow behavior has been addressed by investigations of the effects of slope (Gregg and Fink 2000), slope breaks (Glaze et al. 2014), and

interaction of lava flows with large-scale obstacles (Dietterich et al. 2015). Observations of active flows have shown that topographic features on the order of flow height and less can promote flow divergence and slow flow advance (Hamilton et al. 2013; Dietterich and Cashman 2014). For example, Hon et al. (1994) highlighted the impact of tens-of-centimeter-scale topographic variations on the initial stages of emplacement of sheet flows and pointed out that this influence may later be difficult to identify as flows thicken and inflate. Hamilton et al. (2013) used digital photogrammetry at the active flow fields of Kīlauea volcano, Hawai'i, to create high spatial resolution digital terrain models of pre-flow topography and subsequent path of emplaced basalt flows. They determined that topographic relief 15% or greater than a flow toe's initial thickness may significantly affect flow path, as centimeter-scale topography may deflect or stagnant the progression of pāhoehoe lobe emplacement. However, the influence of fine-scale topography, or bed roughness, on lava flow emplacement, and particularly on flow advance rates, has yet to be investigated experimentally in a systematic manner.

Lava flow mechanics and cooling

When lava flows interact with large-scale topography, that is, when the vertical amplitude of pre-existing topographic variability is comparable to or larger than the flow thickness, H, topographic features have clear influences on flow behavior, acting as natural barriers or culverts to the flow (Fujita et al. 2009; Scifoni et al. 2010; Dietterich and Cashman 2014; Crown and Ramsey 2017). Topographic variability on a scale that is less than that of the flow height is often referred to as "bed roughness," and has subtle influences on flow behavior (Hamilton et al. 2013). Considering fluid dynamics, a substrate with vertical amplitude greater than the thickness of the basal boundary layer of a lava flow may interrupt the internal velocity structure of the flow by creating internal folding and disruptions which could affect flow velocity (Kundu and Cohen 2004; Furbish 1997). This has been shown for ice sheets (Wolovick et al. 2014). Bed roughness with an average amplitude less than the thickness of the flow's basal thermal boundary layer is typically considered hydrodynamically smooth with no direct influence on the velocity structure of the flow (Furbish 1997). However, a rough bed may cause irregular geometries at that boundary as the lava cools through its base. The geometric and temporal scales at which these effects influence lava flow emplacement are unclear. This study is intended to evaluate these scales so that a "roughness factor" can be included in lava emplacement models.

The thermal evolution of a lava flow has a direct influence on flow dynamics, primarily through the control of temperature on lava rheology and through the formation of a crust

(Stasiuk et al. 1993; Keszthelyi and Self 1998; Tarquini 2017). The effective viscosity of lava depends on its temperature and composition, as well as the volume fraction, shape, and size distribution of crystals and bubbles (e.g., Griffiths 2000; Hoover et al. 2001; Giordano et al. 2008), all of which evolve with flow cooling (e.g., Pinkerton and Sparks 1978; Griffiths 2000; Chevrel et al. 2013). A lava flow loses heat primarily through radiation and convection into the atmosphere at its upper crust (e.g., Dragoni 1989; Crisp and Baloga 1990; Harris et al. 1997) and, secondarily, by conduction to the ground (e.g., Hon et al. 1994; Keszthelyi 1995; Rumpf et al. 2013b). Much consideration has been given to the transfer of heat from the upper surface of a flow (e.g., Crisp and Baloga 1990; Harris et al. 1997; Keszthelyi et al. 2003); however, the transfer of heat into the substrate is often overlooked (e.g., Oppenheimer 1991; Keszthelyi and Denlinger 1996; Harris et al. 1997; Keszthelyi and Self 1998) despite evidence that it contributes to a significant and variable portion of heat loss from the flow (e.g., Keszthelyi 1995; Harris et al. 1998; Rumpf et al. 2013a, b). Models of surface flows at Kīlauea volcano and at Okmok volcano, Alaska (Harris et al. 1998; Patrick et al. 2004), showed that conduction of heat into the ground accounts for 10–30% of heat loss from a lava flow, and that this percentage increases with the development of a cohesive surface crust and as radiative heat loss becomes secondary to convective cooling and conduction to the substrate (Keszthelyi et al. 2003). Measurements taken by Keszthelyi (1995) by placing thermocouples in the paths of active lava flows at Kīlauea found that lava-substrate interface temperatures increased rapidly after initial lava emplacement, then plateaued until heating resumed 2 to 4 min after emplacement, an increase inferred to be the expression of latent heat released during the crystallization of microlites in the basalt. The thermophysical properties of the substrate will affect the flux of heat into the substrate (Harris et al. 1998; Patrick et al. 2004) and thereby the internal temperature of the lava flow, which controls flow mobility (Rumpf et al. 2013a).

It is possible that a substrate with larger amplitude of topographic variability will increase the rate of heat loss into the ground by increasing the contact area between lava and substrate as the lava partially fills the void space between small topographic variations. There is field evidence that pāhoehoe flows fill in voids in the underlying substrate (Brown et al. 2015); however, the occurrence rate of such events has not been investigated. For example, Brown et al. (2015) describe an outcrop in the Columbia River Basalts in which a pāhoehoe flow filled in a crack in a tephra fall deposit. In-filling of the substrate has also been observed in pre-historic basaltic outcrops on O'ahu. Figure 1 shows examples of pāhoehoe toes intruding into 'a'ā clinker at Makapu'u, O'ahu. The small size (< 10 cm, in places) of the intruding toes indicates that the lava had a low viscosity during emplacement.
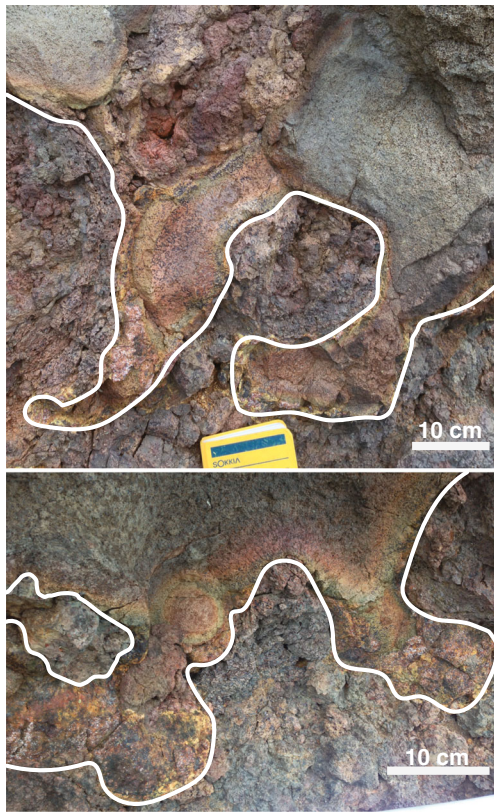
Fig. 1 Toes of a pāhoehoe lava flow intruding into the upper clinker layer of an underlying 'a'ā lava flow. White lines indicate contacts between units. Photographs are from an outcrop of prehistoric basalt flows at Makapu'u Point on the island of O'ahu, Hawai'i

Motivation

One of the central goals of volcanology is to provide models that predict lava flow advance rates and inundation zones, which serve as the basis for hazard estimation and preparation for communities in volcanic areas (e.g., Harris and Rowland 2001, 2015; Rowland et al. 2005). Residents and policy makers in and around zones of volcanic hazard benefit greatly from the availability of information regarding potential eruption impacts, including estimations of lava emplacement timelines and maps of predicted lava flow paths and inundation zones (Scott 1989; Behncke et al. 2005; Ganci et al. 2012; Harris and Rowland 2015). Examples of popular flow prediction tools include the thermo-rheological model FLOWGO (Harris and Rowland 2001, 2015), the cellular automata code MAGFLOW (Cappello et al. 2015), and the probabilistic tool DOWNFLOW (Favalli et al. 2005; Tarquini and Favalli 2011), as well as more complex fluid-mechanics models such as LavaSIM (Hidaka et al. 2005; Proietti et al. 2009) and codes based on smooth-particle hydrodynamics (SPH; Herault et al. 2011). Most existing lava flow models consider the effects of large-scale topography and surface slope on flow path (see Cordonnier et al. 2015 and Dietterich et al. 2017 for model comparisons), but not substrate roughness. A critical input

parameter to DOWNFLOW, dh, is the amount of variation of a given digital elevation model between iterations of the model. Arguably, dh represents the effect of small-scale topography indirectly (Favalli et al. 2011; Richter et al. 2016). However, this single parameter is also supposedly accounting for DEM uncertainty and flow widening and branching, and there is no formal way to convert from observed topographical roughness to dh. Thus, to date, no model includes the effects of fine-scale topography (less than typical flow height) on flow path and mobility formally and thorough quantitative assessment of the bed roughness. Other substrate characteristics, such as vegetation, cohesion, and moisture content, are also not yet included in existing emplacement models, but can be, for example, relations have been developed for mechanical erosion of the substrate by a lava flow (Ferlito and Siewert 2006; Siewert and Ferlito 2008). Exclusion of these parameters has been the result of lack of observational constraints and simple, adaptable formulations, and sometimes the assumption that they will have a minimal influence on flow emplacement. In addition, substrate properties are excluded from flow models due to limited data availability. A quantitative characterization of pre-existing fine-scale topography, cohesion, and vegetation cover is not regularly performed for volcanic areas. However, new and improved satellite observations and techniques such as manned and unmanned aerial photogrammetry and airborne laser altimetry now produce significantly high-resolution topography datasets (i.e., < 10 cm vertical and horizontal resolution) at volcanic areas (e.g., Tarolli 2014; Müller et al. 2017; Turner et al. 2017). Such datasets allow for quantitative substrate characterization and can potentially be included in forward models of flow emplacement in the near future (Cashman et al. 2013; Whelley et al. 2014).

Past experimental work

The use of analog materials in a laboratory setting is a well-established method in the investigation of lava flow dynamics (e.g., Fink and Griffiths 1990; Blake and Bruno 2000; Dietterich et al. 2015). Analog experiments allow for adjustment of experimental parameters in a safe and predictable environment. For this study, we chose three materials that have been previously utilized by volcanologists to study lava flow emplacement: corn syrup, polyethylene glycol (PEG), and molten basalt. We review past experimental work that used these materials, and their known properties, in the following sections.

Corn syrup is a Newtonian fluid with a viscosity dependent on its composition (sugar content) and temperature, similar to magmatic melts (e.g., Stasiuk et al. 1993; Soule and Cashman 2005; Castruccio et al. 2010). Corn and similar sugar-based syrups have recently been used to simulate the interaction of lava flows with obstacles (Dietterich et al. 2015). PEG is a Newtonian fluid capable of solidifying at temperatures easily

attainable in the laboratory (~ 18 °C, and can thus form a brittle crust and morphologies similar to advancing lava flows (e.g., Fink and Griffiths 1990; Blake and Bruno 2000; Kerr et al. 2006). Previous studies using PEG have revealed that substrate roughness has effects on PEG behavior and emplacement (e.g., Bridges 1992; Griffiths and Fink 1992; Gregg and Fink 1996; Gregg and Fink 2000). Principally, a rough base provides a no-slip condition at the flow-substrate boundary, which is necessary to appropriately simulate flow emplacement. Fink and Griffiths (1990) found that the addition of a 3- to 4-mm mesh to the emplacement surface of their experimental apparatus reduced basal slip, thereby decreasing downslope and lateral spreading while increasing compressive stresses within the flows, resulting in realistic lava-like flow morphologies. Furthermore, experiments by Fink and Griffiths (1992) found that increasing the friction at the fluid-substrate boundary modified the conditions at which morphological transitions occurred. In addition, Bridges (1992) and Fink et al. (1993) completed experiments using a surface with positive topographic elements with ~ 1 cm spacing and ~ 1 cm vertical relief, which resulted in PEG flows much thicker than in experiments using a wire mesh with fine spacing and little vertical relief.

The direct measurement of lava–substrate interactions in natural settings is dangerous and logistically difficult, the results of Keszthelyi (1995) being a rare exception. The authors could find no papers since Keszthelyi (1995) that report on direct measurements at the base of an active lava flow. Using molten basalt in controlled experiments solves these problems and provides the advantage of capturing lava behavior at temperature and viscosities that reflect natural conditions (e.g., Edwards et al. 2013; Rumpf et al. 2013b; Dietterich et al. 2015). Experiments by Rumpf et al. (2013b) directly measured the heat transfer from molten basalt into the underlying substrate. For each experiment, a container was partially packed with particulate material and embedded with thermocouples before being filled with molten basalt at ~ 1200 °C. The insulating nature of the particulate material impeded efficient heat transfer into the substrate indicating that substrate material can affect heat loss from a lava flow (Rumpf et al. 2013b). Similar experiments were conducted at the Syracuse University Lava Project facilities (http://lava-dev.syr.edu/) in which molten basalt was poured over substrates of layered water-ice and sand (Edwards et al. 2013). Measurements of substrate temperatures during the experiment indicated delayed heating of ice layers when buffered by an overlying sand layer.

Experimental procedures

We conducted three sets of laboratory experiments to simulate the emplacement of lava onto a rough substrate. Each set of experiments used a different fluid: corn syrup, PEG, or molten basalt, to capture a different aspect of lava rheology. In each experiment, the liquid was extruded onto a sloping plane covered by a continuous layer of particles of a specific size. We describe below the materials and experimental setups for each of the three sets of experiments. Experimental conditions and material properties are summarized in Tables 1 and 2.

Corn syrup and polyethylene glycol experiments

Two sets of analog experiments were completed, one used corn syrup and the other used PEG. The experiments were designed and completed at the new Fluid Mechanics laboratory at the Lamont-Doherty Earth Observatory (LDEO) at Columbia University. The experimental setup (Fig. 2) included a rigid plexiglass plane tilted at 7°, interchangeable plastic boards covered with particles of varying grain sizes, a speed-adjustable peristaltic pump (Masterflex™ 77600-62), and a fluid reservoir.

Substrates with a range of topographic variability length scales were placed on top of the sloping plane. Rough surfaces were constructed by either using sand paper of various grits or by gluing continuous layers of particles of different sizes, referred to hereafter as the substrate *mean grain size* (*GS*). The mean grain size of the particles dictated both the horizontal particle spacing and the vertical amplitude of the roughness. Substrates used for both corn syrup and PEG experiments included sand paper with φ (Krumbein grain size scale) values of 3.1, 1.9, and 0 ($\varphi = \log_2(GS)$, with *GS* in mm), corresponding to *GS* of 0.12, 0.27, and 1.0 mm (respectively referred to as grit 120, 60, and 20), and a gravel layer, with a *GS* of 1.0 cm ($\varphi = -3.3$, Table 2).

Corn syrup was diluted with water to a concentration of 73% sugar, which resulted in a viscosity of ~ 7.0 Pa s at room temperature (~ 24 °C). CARBOWAX™ PEG-600 (molecular weight of ~ 600 g/mol) produced by DOW Chemical Company has a viscosity of 1.0 Pa s at room temperature and a solidification temperature of 18 °C. Both analog materials were extruded at room temperature (~ 24 °C). For PEG experiments, the sloped surface was placed into a $100 \times 50 \times 50$ cm plexiglass tank filled with water chilled to ~ 5 °C. We note that in previous experiments (e.g., Fink and Griffiths 1990; Gregg and Fink 1996, 2000), PEG was extruded either into fresh water (Blake and Bruno 2000; Kerr et al. 2006) or into aqueous saline (Fink and Griffiths 1990; Cashman et al. 2006), which more closely replicate lava flow cooling time scales when studying flow regime transitions. We chose to extrude the PEG into fresh water, which helped keep the experiments simple, since the experiments are compared to each other in a relative sense and absolute timescales were of secondary interest. The corn syrup was pumped into open air at a constant flux of 3–4 cm^3/s and the PEG was extruded into the

Table 1 Material parameters

Parameter	Symbol	Units	Basalt	PEG	Corn syrup	Exp. 51[a]	Mauna Loa 1984[b]	Kilauea 1974[c]
Flow material properties								
Velocity	U	m s^{-1}	0.0068	0.0026	0.0036	0.010	2.4	8.3
Max. surface velocity	$U_{\max}$	m s^{-1}	0.0068	0.0026	0.0036	0.010	2.4	8.3
Density	ρ	kg m^{-3}	2700	1120	1400	1127	2000	900
Flow width	L	m	0.60	0.32	0.26	0.30	45	7.8
Flow thickness	H	m	0.06	0.008	0.43	0.010	5.0	2.6
Dynamic viscosity	η	Pa s	150	1.0	7	0.14	12,000	110
Thermal diffusivity	α	m^2 s^{-1}	2.20×10^{-7}	8.00×10^{-9}	5.9×10^{-9}	7.95×10^{-9}	2.20×10^{-7}	2.20×10^{-7}
Heat capacity	C_p	J kg^{-1} K^{-1}	1200	2500	3200	2500	1200	1200
Thermal conductivity	k	W m^{-1} K^{-1}	0.026	0.022	0.026	0.022	0.53	0.24
Solidification temperature	T_s	K	1073	291	273	291	1073	1073
Emissivity	ε	–	0.95	0.90	0.85	0.90	0.98	0.98
Ambient material properties								
Ambient density	ρ_a	kg m^{-3}	1.2	1000	1.2	1003	1.2	1.2
Ambient thermal expansion coefficient	α	K^{-1}	3.40×10^{-3}	3.60×10^{-3}	3.40×10^{-3}	3.60×10^{-3}	3.40×10^{-3}	3.40×10^{-3}
Ambient thermal diffusivity	κ	m^2 s^{-1}	2.15×10^{-5}	1.40×10^{-7}	2.15×10^{-5}	1.4×10^{-7}	2.15×10^{-5}	2.15×10^{-5}
Ambient dynamic viscosity	η	Pa s	1.54×10^{-5}	6.15×10^{-5}	1.54×10^{-5}	6.15×10^{-5}	1.54×10^{-5}	1.54×10^{-5}
Ambient heat capacity	c_a	J kg^{-1} K^{-1}	1010	4100	1010	4100	1010	1010
Average experimental conditions								
Gravitational acceleration	g	m s^{-2}	9.8	9.8	9.8	9.8	9.8	9.8
Stefan-Boltzmann constant	σ_b	W m^{-2} K^{-4}	5.67×10^{-8}	5.67×10^{-8}	5.67×10^{-8}	5.67×10^{-8}	5.67×10^{-8}	5.67×10^{-8}
Flux	Q	m^3 s^{-1}	45.0	7.58×10^{-6}	3.67×10^{-6}	3.64×10^{-6}	50	40
Eruption temperature	T_e	K	1373	296	298	296	1373	1373
Ambient temperature	T_a	K	298	278	298	277	298	298
Normalized eruption temperature	Θ_e	–	1.0	16	–	15	1.00	1.00
Normalized ambient temperature	Θ_a	–	0.28	15	–	15	0.28	0.28
Strain rate	U/H	s^{-1}	0.11	0.33	8.3×10^{-3}	1.0	0.47	3.2
Non-dimensional numbers								
Reynolds number	$\rho U L/\eta$	–	0.074	6.1	0.19	24	18	530
Péclet number	LU/α	–	1.9×10^4	1.0×10^5	1.6×10^5	3.8×10^5	4.8×10^8	2.9×10^8
Froude number	$U/\sqrt{(Hg)}$	–	8.9×10^{-3}	9.3×10^{-3}	1.7×10^{-3}	0.032	0.34	1.6
Flow regime parameter	Ψ	–	2060	2.24	–	12.20	32.80	118.00

[a] Fink and Griffiths (1990)

[b] Moore (1987)

[c] Heslop et al. (1989)

water at 7–8 cm^3/s. Thermocouples recorded water temperatures during PEG experiments. All experiments were recorded from above by a high-definition video camera and by digital still cameras looking horizontally at the flow side and flow front (Fig. 2).

Our PEG experiments were designed to fit within specific regimes of a key non-dimensional parameter used frequently to describe the dynamics of lava flows. This "flow regime parameter", Ψ (Fink and Griffiths 1990; Gregg and Fink 2000; Gregg and Keszthelyi 2004), is equal to the ratio between t_s, the time it takes to form a crust at the flow surface, and t_a, the time a flow takes to advance a distance equal to its thickness. It has been shown that certain values of Ψ mark the transition between flow regimes and morphologies. For flows on a smooth surface, such as those conducted by Fink and Griffiths (1990), flow regimes are defined by the following: pillows at $\Psi < 0.65$, rifted flow at $0.65 < \Psi < 2.8$, folded flows at $2.8 < \Psi < 6.5$, and channelized flows at $\Psi > 6.5$. For a flow on a wire mesh base (that is, no slip basal boundary condition), Gregg and Fink (2000) found that high values of Ψ (> 30) correspond to disrupted flow structures and surfaces, leading to a channelized,

Table 2 Experimental results

Exp. no.	Substrate material	Grain size range[a] (cm)	Grain size range[a] (φ)	Mean grain size (cm)	Slope (°)	Material density (kg m⁻³)	Pour time (s)	Flow emplacement time (s)	Pour mass (kg)	Final average thickness (cm)
Corn syrup										
1	Gravel	0.3–1.3	−1.7 to −3.7	1.0	7	1400	356	351	1.722	0.50
2	Gravel	0.3–1.3	−1.7 to −3.7	1.0	7	1400	486	481	1.979	0.50
3	SP - Grit 20	0.1	0	0.10	7	1400	184	186	0.911	0.35
4	SP - Grit 20	0.1	0	0.10	7	1400	192	191	0.850	0.35
5	SP - Grit 60	0.027	1.9	0.027	7	1400	158	161	0.951	0.45
6	SP - Grit 60	0.027	1.9	0.027	7	1400	170	171	0.875	0.40
7	SP - Grit 120	0.012	3.1	0.012	7	1400	154	156	0.814	0.50
8	SP - Grit 120	0.012	3.1	0.012	7	1400	141	141	0.894	0.40
PEG										
1	Gravel	0.3–1.3	−1.7 to −3.7	1.0	7	1120	230	355	1.980	0.79
2	Gravel	0.3–1.3	−1.7 −−3.7	1.0	7	1120	300	355	2.601	1.1
3	Gravel	0.3–1.3	−1.7 to −3.7	1.0	7	1120	300	375	2.715	0.72
4	SP - Grit 20	0.1	0	0.10	7	1120	195	245	1.471	0.91
5	SP - Grit 20	0.1	0	0.10	7	1120	240	375	2.100	–
6	SP - Grit 60	0.027	1.9	0.027	7	1120	180	265	1.548	0.93
7	SP - Grit 60	0.027	1.9	0.027	7	1120	180	165	1.467	0.79
8	SP - Grit 120	0.012	3.1	0.012	7	1120	180	275	1.570	0.81
9	SP - Grit 120	0.012	3.1	0.012	7	1120	180	185	1.499	0.85
Basalt										
1	Cobble	3.8–8.5	−5.3 to −6.4	6.4	9.7	2700	116	186.1	38.22	5.0
2	Coarse gravel	1.9–3.8	−4.3 to −5.3	2.9	8.8	2700	93	88.1	34.56	3.8
3	Med. lava rock gravel	0.6–4.1	−2.7 to −5.4	1.9	9.3	2700	103	82.1	29.48	3.8
4	Med. gravel	1.3–1.9	−3.7 to −4.3	1.6	8.75	2700	126	152.1	38.90	4.7
5	Fine gravel	0.6–1.3	−2.7 to −3.7	1.0	9.50	2700	85	130.1	22.79	4.9
6	V. fine gravel	0.1–0.6	−0.3 to −2.7	0.48	9.5	2700	63	147.1	19.16	3.0

Exp. no.	$R = GS/H$	Final maximum width (cm)	Final length (cm)	Flux—volume (cm³ s⁻¹)	Final surface area (cm²)	Final perimeter (cm)	Perimeter factor	Average velocity (cm s⁻¹)
Corn syrup								
1	2.0	36.4	65.7	3.46	1710	414	7.03	0.19
2	2.0	45.0	68.5	2.91	2020	368	5.00	0.14
3	0.29	19.3	65.4	3.54	1320	169	1.05	0.35
4	0.29	19.7	69.7	3.16	1250	166	1.03	0.36
5	0.060	26.5	69.7	4.30	1500	171	1.12	0.43
6	0.068	22.4	69.2	3.68	1360	166	1.05	0.40
7	0.024	18.9	71.6	3.78	1210	164	0.99	0.46

**Table 2** (continued)

Exp. no.	$R = GS/H$	Final maximum width (cm)	Final length (cm)	Flux—volume (cm³ s⁻¹)	Final surface area (cm²)	Final perimeter (cm)	Perimeter factor	Average velocity (cm s⁻¹)
8	0.030	21.3	69.7	4.53	1320	165	1.02	0.49
PEG								
1	1.3	30.1	72.8	7.69	1580	268	2.75	0.21
2	0.91	36.1	68.3	7.74	1810	278	2.93	0.19
3	1.4	33.1	76.5	8.08	1690	304	3.40	0.20
4	0.11	29.1	75.9	6.74	1560	239	2.12	0.31
5	–	29.4	69.2	7.81	1500	257	2.70	0.18
6	0.029	32.3	69.4	7.68	1520	246	2.57	0.26
7	0.034	29.5	58.0	7.28	1230	200	2.19	0.35
8	0.015	35.0	68.7	7.79	1590	253	2.71	0.25
9	0.014	33.8	67.6	7.44	1390	217	2.28	0.37
Basalt								
1	1.3	58.3	98.6	122.03	3910	342	2.15	0.53
2	0.76	68.8	71.3	137.63	4240	286	1.54	0.81
3	0.50	59.8	70.5	106.01	4000	279	1.53	0.86
4	0.34	63.9	107.8	114.34	4540	294	1.37	0.71
5	0.20	54.4	74.3	99.30	3300	222	1.14	0.57
6	0.16	54.1	90.0	112.64	4550	265	1.11	0.61

R roughness factor, GS average substrate grain size, H final average thickness, SP sandpaper

[a] Ranges were not determined for SP. Mean grain sizes are based on Coated Abrasives Manufacturers Institute standards

Fig. 2 Schematic of the experimental setup for corn syrup and polyethylene glycol (PEG) experiments at Columbia University. Corn syrup experiments were performed in open air without the use of water tank
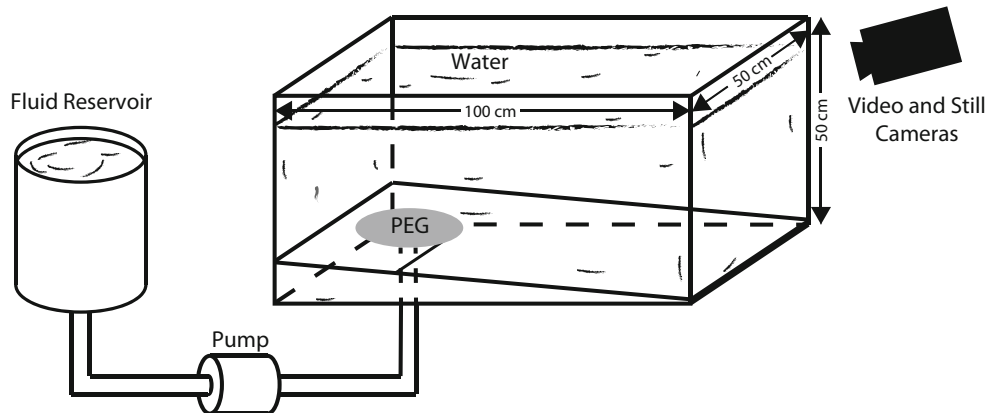
leveed flow. Folded flows, similar to ropy pāhoehoe, are expected when $13 < \Psi < 30$. Rifted flows occur when $3 < \Psi < 13$ and are characterized by slabs of solid crust floating above a liquid interior. The lowest Ψ values (< 3) correspond to lobate and pillowed flows (Gregg and Fink 2000).

Our experiments reside in the "levéed" and "folding" regimes of the Ψ parameter (Table 1). Similarly to most natural lava flows, all experiments were in the laminar flow regime (large Reynolds numbers) and were advection-dominated, as evident by the large Péclet numbers (Table 1). PEG flows were "volume limited" in that the extrusion of material stopped before the flow reached its maximum length.

Molten basalt experiments

Experiments with molten basalt were performed at the Syracuse University Lava Project facility. The facility includes a gas-fired tilting furnace capable of melting up to 350 kg of basalt at over 1200 °C and maintaining temperature for over 24 h (Fig. 3). The flow bed was made of a steel sheet sloped at 8.5–10°, ~2 m wide, and ~3 m long, which was covered with a 5–10 cm layer of sand followed by a range of substrate materials: basalt chips ($GS = 0.48$ cm, $\varphi = -2.3$) and sandstone pebbles of increasing size ($GS = 1.0, 1.6, 1.9, 2.9$, and 6.4 cm, $\varphi = -3.3, -4, -4.2, -4.9$, and -6.0) (Table 2). Basalt was poured onto each of the beds at a flux of ~100 to 140 cm^3/s through a chute for 1 to 2 min. Temperature, and therefore viscosity, differences between the molten basalt samples during different pours did not allow for exact replication of fluxes. Two still cameras collected time-lapse images of the flows from both sides of the setup and a high-definition video camera looking straight down recorded flow emplacement from ~2 m above the flow surface (Fig. 3). A thermal video camera (FLIR Model SC325), co-located with the visible video camera, and thermocouples, placed at the lava-substrate boundary and within the substrate, monitored the surface and basal temperatures, respectively, during emplacement and cooling of each run.

Analysis

For each set of experiments, video recordings and still images were used to determine flow velocities and morphologies. Still image sequences were created from the overhead video. Flow lengths as a function of time were measured as the furthest distance of continuous flow from the center of the vent (or the end of the pour chute, for basalt) by automated Matlab™
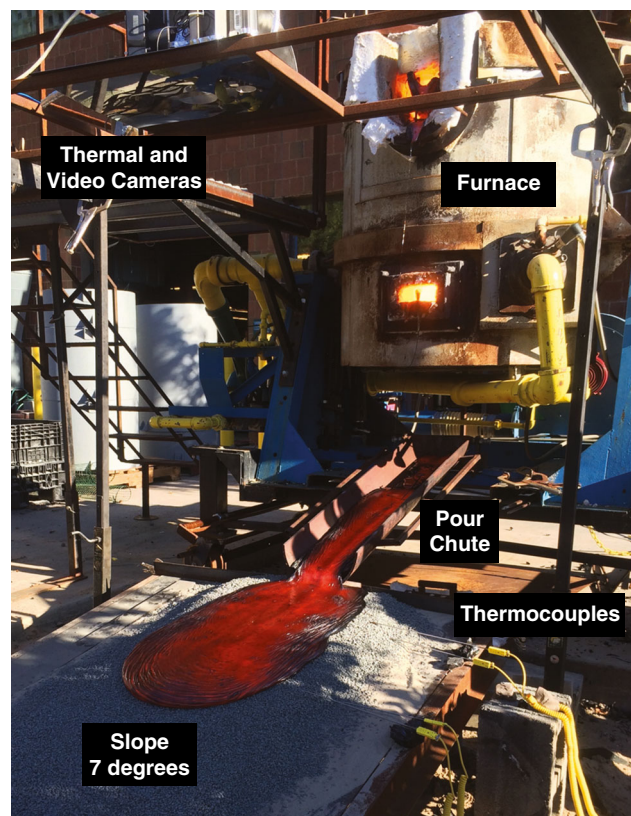

Fig. 3 Furnace and experimental setup at the Syracuse University (SU) Lava Project facility. Lava pours from the furnace, down a metal chute, and onto a surface covered in substrate material and sloped in between 9° and 10°. Thermocouples were placed at the lava–substrate boundary and at ~5 cm depth within the substrate. Overhead thermal and video cameras record experiments

scripts. Maximum flow widths were measured from the overhead sequence images as the maximum straight-line distance of continuous material emplacement perpendicular to the downslope direction. Flow thicknesses were determined using the side view still images, by caliper after flow motion ceased for corn syrup and PEG flows, and by direct measurement of the solidified basalt during flow disassembly. In addition, we developed a *perimeter factor* to characterize the final shape of each flow. This factor is a ratio of the length of the perimeter squared divided by the final area of the flow normalized to the perimeter squared divided by the surface area of a perfect ellipse with the same maximum width and length as the flow. For flows with similar width/length ratios, a higher perimeter factor indicates a more irregular flow boundary geometry. A perfectly smooth oval shape will have a perimeter factor of 1.

Results

Still images of experiments are presented in Figs. 4, 5, and 6, for corn syrup, PEG, and molten basalt, respectively. Videos of experiments are available as Online Resources 1–7. Experimental results are summarized in Table 2 and displayed in Figs. 7, 8, and 9.
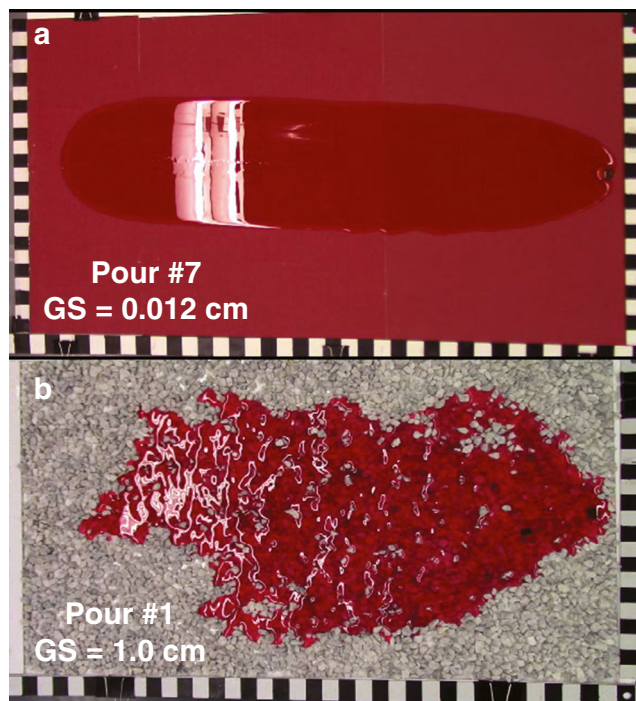
Fig. 4 Overhead stills of corn syrup (red) flows during experimental emplacement. **a** Pour 7 onto substrate with $GS = 0.012$ cm, image captured 142 s after experiment initialization. **b** Pour 1 onto substrate with $GS = 1.0$ cm, image captured 306 s after experiment initialization. Corn syrup was extruded from a vent on the right of image onto 7° slope. Each mark on scale bar represents 2 cm
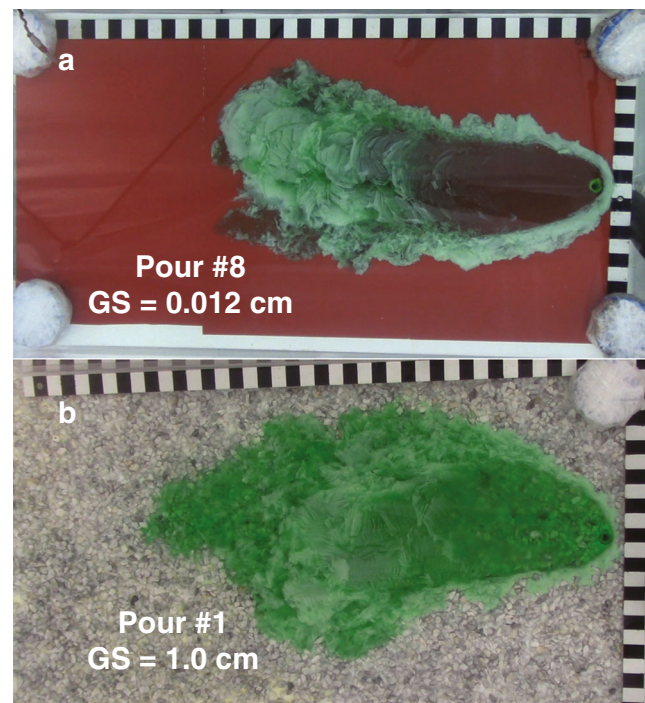

Fig. 5 Overhead photographs of polyethylene glycol (PEG, green) flows during experimental emplacement. **a** Pour #8 onto substrate $GS = 0.012$ cm, image captured 160 s after experiment initialization. **b** Pour #2 onto substrate $GS = 1.0$ cm, image captured 280 s after experiment initialization. PEG was extruded from a vent on the right of image onto 7° slope. Each mark on scale bar represents 2 cm

Corn syrup

Corn syrup experiments onto substrates with grain sizes between 0.012 and 0.10 cm (runs 3–8, Table 2) had similar symmetric, oval outlines advancing downslope from a central flow front (Fig. 4a, Online Resource 1). Experimental emplacement onto the $GS = 1.0$ cm substrate (runs 1 and 2, Table 2) displayed irregular outlines and advanced from multiple lobes as gravel pieces locally diverted the flow (Fig. 4b, Online Resource 2). Perimeter analysis found very similar flow shapes for each of the runs emplaced onto sandpaper, each with perimeter factors between 0.99 and 1.12 (Fig. 7, Table 2). Flows 1 and 2, both emplaced on gravel ($GS = 1.0$ cm), had perimeter factors of 7.03 and 5.00, respectively, representing seven and five times the complexity of the runs on surfaces with smaller grain sizes. Average flow thicknesses varied between 0.35 and 0.50 cm with no significant correlation to substrate grain size (Table 2). Maximum flow widths increased from roughly 0.2 m for all $GS = 0.012$ to 0.1 cm to roughly 0.4 m for $GS = 1.0$ cm substrate.

For corn syrup on all substrate types, downslope flow front velocities peaked immediately after initiation of the experiment and decreased with time (Fig. 9a). Initial flow velocities were greatest on the smoothest substrate (~ 1.1 m/s on $GS = 0.012$ cm) and the lowest on the roughest substrate (~ 0.6 cm/s on $GS = 1.0$ cm). At all times, flow front velocities decreased

Fig. 6 Overhead photographs of molten basalt flows during experimental emplacement. **a** Pour #6 onto substrate $GS = 0.48$ cm, image captured 34 s after experiment initialization. **b** Pour #5 onto substrate $GS = 1.0$ cm, image captured 83 s after experiment initialization. **c** Pour #2 onto substrate $GS = 2.9$ cm, image captured 76 s after experiment initialization. **d** Pour #1 onto substrate $GS = 6.4$ cm, image captured 70 s after experiment initialization. Basalt was poured from furnace via chute at left of images onto substrate surfaces with slopes in between 9° and 10°
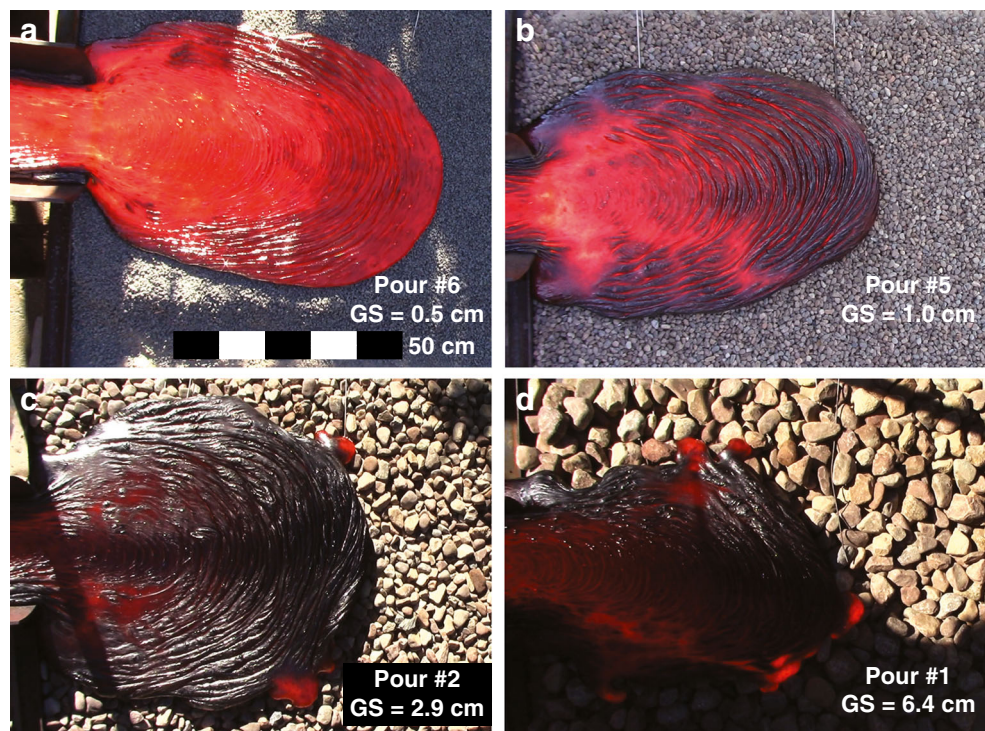
with increasing substrate grain size. This trend continued, but diminishing with time, after the initial onset of the experiments. Faster flow front advance rates led to shorter total experiment times for runs with finer substrates (Fig. 8a).

Polyethylene glycol

For all substrate types, PEG flows were oval-shaped with increasing width downslope (Fig. 5, Online Resources 3 and 4). Each flow developed lobate margins and a central levéed channel (Fig. 5) as the PEG cooled and solidified. Flows tended to advance downslope from one central flow front; however, multiple flow fronts advancing at similar rates were observed. All PEG flows had perimeter factors between 2.12 and 3.4 (Fig. 7, Table 2). There is a slight increasing trend in the perimeter factor with increasing grain size, with an average perimeter factor for flows on $GS = 0.012$ cm of 2.50 and an average perimeter factor for flows on $GS = 1.0$ cm of 3.03. Average flow thicknesses varied between 0.7 and 1.0 cm and maximum flow widths ranged from 0.29 to 0.36 m, with no correlation between flow thickness or width and GS (Table 2).

For PEG on all substrates, flow front advance rate was greatest immediately after experiment start and gradually decreased with time (Fig. 9b). Initial flow front velocities were greatest on the finest substrate (~ 1.5 cm/s on $GS = 0.012$ cm) and lowest on the coarsest substrate (~ 1.0 cm/s on $GS = 1.0$ cm). The average flow front velocities decreased as substrate grain size increased for all times. The differences

between flow front velocities for the different grain-sized substrates decreased with time. Flows on the three finer substrate sizes reached their final lengths of 0.58 to 0.75 m in roughly 175 s, while the gravel substrate took ~ 360 s to attain final lengths of 0.68 to 0.76 m.

Molten basalt

For most substrate types, the basalt flows maintained nearly symmetric oval outlines with major axis parallel to the slope. All the flows had a ropey pāhoehoe texture and advanced downslope along a broad flow front (Fig. 6, Online Resources 5–7). Three of the six flows presented here produced breakouts near the flow front. There is a clear increase in perimeter factor with increasing grain size for the molten basalt pours (Fig. 7, Table 2). The perimeter factor is 1.11 and 1.14 for the two finest substrates ($GS = 0.5$ and 1.0 cm) and increases to 2.15 for the coarsest substrate (6.4 cm). The increasing complexity of the basalt flow margins with increasing grain size is distinctive in images (Fig. 6). For example, run 6 is onto a substrate with $GS = 0.5$ cm and displays smooth edges (Fig. 6a); run 2, onto $GS = 2.9$ cm, develops scalloped edges on the order of 20 cm (Fig. 6b); and flow 1, onto $GS = 6.4$ cm, is highly irregular with multiple breakouts in several directions and little symmetry (Fig. 6d). Average basalt flow thicknesses were scattered between 3.0 and 5.0 cm and maximum flow widths varied between 54 and 69 cm with no correlations with grain size (Table 2).
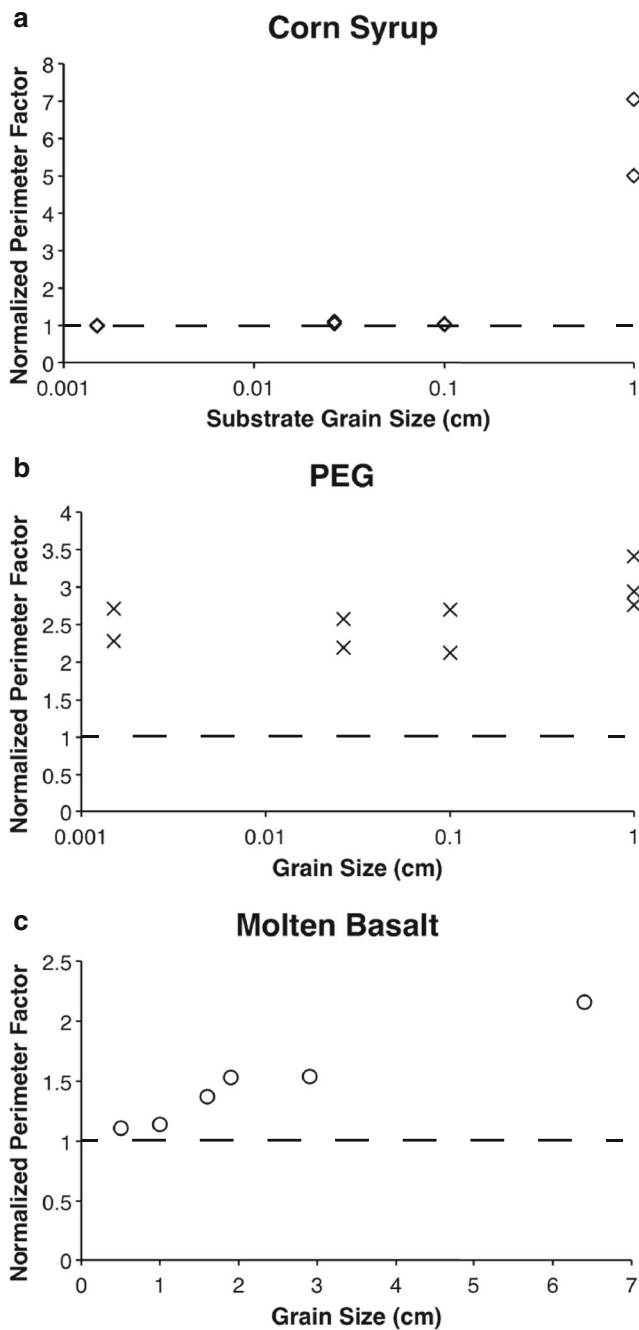
Fig. 7 Flow perimeter values versus mean substrate grain size for **a** corn syrup, **b** polyethylene glycol (PEG), and **c** molten basalt. For each material, the normalized perimeter factor increases with increasing substrate grain size. Flow perimeter lengths and areas were measured after movement of flows ceased. Dashed lines indicate perimeter factor for perfect ellipse

Fig. 8 Flow length with time after experiment initialization for **a** corn syrup, **b** polyethylene glycol (PEG), and **c** molten basalt. Markers represent experimental measurements. Lines represent analytical solutions for the advance of a Newtonian fluid with a given effective viscosity on a slope and at a flow thickness equal to the experimental conditions

Flow front velocities were highest immediately after experiment start and decreased with time consistently throughout each experiment (Figs. 8c and 9c). The highest initial velocity of ~ 6.8 cm/s occurred on the 1.0 cm *GS* substrate (i.e., the second finest substrate), and the slowest initial velocity of ~ 2.2 cm/s occurred on the largest (*GS* = 6.4 cm) grain-sized substrate (Fig. 9c). In general, flow front velocities at any given point in time decreased with increasing mean grain size; however, this trend was not as clear as in the analog experiments. This trend is well-defined early in experimental runs and decreases with time after initial emplacement, with velocities on different substrates becoming almost indistinguishable after 60 s (Fig. 9c).

Discussion

Our experiments show that fine-scale topography of the underlying substrate impacts the advance rate and shape of basalt and analog fluid flows. For corn syrup and PEG experiments,
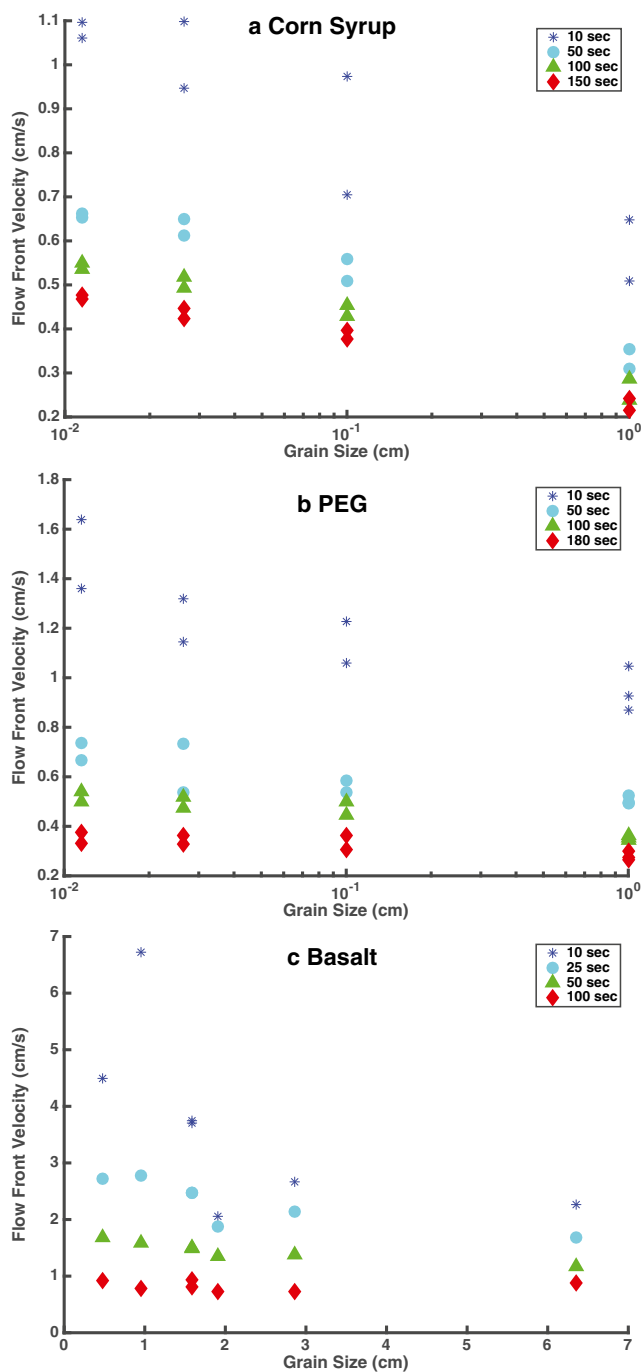
Fig. 9 Experimental flow front advance rates versus mean substrate grain size with time for **a** corn syrup, **b** polyethylene glycol (PEG), and **c** molten basalt. Flow advance rates decrease with increasing substrate grain size. This trend decreases with time after experiment start

clear relationships show that flow front velocity decreases with increasing substrate grain size. This trend diminishes with time within the scale of experiments. For basalt experiments, initial flow front velocity decreases with increasing grain size, but with time, the velocities for all substrate types become nearly indistinguishable. Both molten basalt and corn syrup show distinct changes in flow morphology when

emplaced on substrates of different grain sizes. Coarser substrates produced irregular flow shapes and encouraged the development of breakouts and movement of material laterally, instead of an idealized oval spreading primarily downslope.

Our results demonstrate that topography at amplitudes that are similar to or less than flow thickness can significantly reduce advance rate at the early stages of flow emplacement. We explain this through two primary mechanisms: one based on mechanical influences of the substrate geometry and one a result of thermal interactions between the lava and the substrate. Coarse substrates, particularly when unsorted and poorly packed, as is often the case in nature, have large void spaces. Fluid emplaced on top of such substrates will penetrate into these void spaces. This will act to slow down advancement of the flow as material moves downward instead of only forward and laterally. This process was apparent in the analog pours (corn syrup and PEG experiments) on substrate of $GS =$ 1.0 cm as material could be seen moving into void spaces. For basalt pours on coarse substrates, post-experiment examinations of the basalt–substrate interface revealed irregular surfaces, with the basalt inundating the substrate, moving between and often incorporating the substrate rocks into the base of the flow (Fig. 10). Natural examples of lava penetrating into pre-existing topographic voids exist as well (e.g., Fig. 1). Thermally, a coarse topography with larger void spaces implies a larger contact area between the flow and the substrate, provided the lava at least partially fills the void spaces. Since the rate of heat loss by conduction into the substrate depends on the surface area (Carslaw and Jaeger 1959), an increased surface contact area means a more efficient and faster cooling of the flow. For fluids with a temperature-dependent viscosity such as lava, faster cooling then causes a higher viscosity and a slower flow.

These mechanical and thermal interactions also explain the diminishing influence of substrate roughness on the flow advance rate at later stages of the flow emplacement. Fluid arriving behind the flow front is advancing over a basal boundary layer that has already developed at the fluid–substrate interface and decreases the influence of substrate type. This layer provides mechanical buffering, because voids have already been partially or completely filled, and thermal insulation, because movement over a basal layer of lava will provide a smaller temperature gradient than movement over a substrate at ambient temperature. In addition, the flow front will cool and became more viscous or solidify with time. A more viscous flow front is less sensitive to the roughness as it is less capable of filling in the small void spaces. The development of a boundary layer and an increase in fluid viscosity is likely to occur quickly after initial flow emplacement because the initial temperature gradient between the flow and a substrate at ambient temperature is very high and the flow will rapidly lose heat to the substrate (Keszthelyi 1995; Keszthelyi and Denlinger 1996).
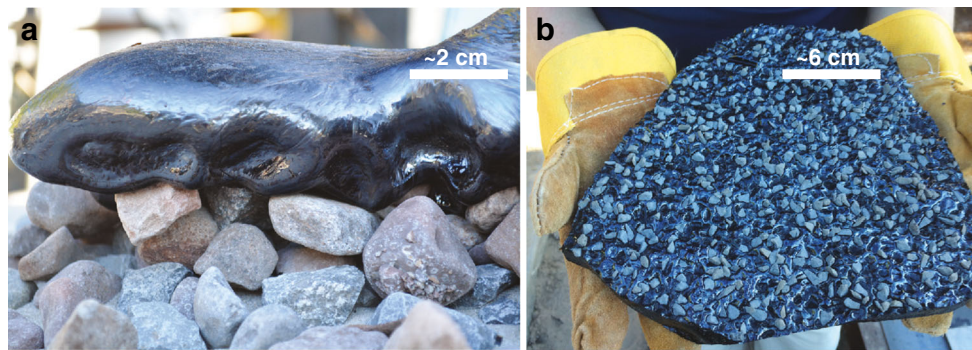
Fig. 10 Photographs from molten basalt pours #2 (**a**) and #6 (**b**) displaying flow interaction with substrate. During pour #2 (**a**, image looking laterally at flow edge), the basalt flowed in between substrate grains. Removal of the substrate revealed indents in the bottom crust of the flow where substrate grains were located during emplacement. During pour #6 (**b**), some substrate grains were affixed to the bottom of the flow while others detached freely and left indents where they were located during flow emplacement

Scaling to natural flow advance rate

Projecting the results of this study to natural lava flows requires scaling our experiments to natural length and time scales of active flows. Two key length scales in our experiments were the vertical amplitude of the bed roughness, expressed by the mean grain size used (GS) and the flow thickness (H). Therefore, we express the influence of bed roughness on flow advance as a function of the ratio, R, where $R = GS/H$. For the experiments presented here, R ranged from 0.014 to 2.0 (Table 2). In nature, these ratios correspond to substrates ranging from very coarse sand ($\varphi = -1$) to cobbles ($\varphi = -6$) for 10-cm-thick pāhoehoe toes. For a ~1.0-m-thick pāhoehoe flow, these reflect the range from pebbles ($\varphi = -5$) to boulders ($\varphi > -8$). For a thicker (5 m) basaltic 'a'ā flow (e.g., those at Mt. Etna, see Walker 1967), these ratios reflect, at their highest values, large boulders ($\varphi > -8$). For even thicker flows, such as those at Okmok (30–50 m, Lu et al. 2005), $0.014 < R < 2.0$ corresponds to topographic features with significant heights such as large boulders to significant hills.

The key time scales in our experimental and natural lava flows are those of radiative, convective, and conductive cooling, of solidification, and of advection (set by flow velocity and volumetric flux). Similarity between analog and natural systems is commonly demonstrated through similarity in the ratios between these time scales, expressed as non-dimensional numbers. Table 1 displays values for non-dimensional numbers relevant to the cooling and advection timescales. The Reynolds number (Re), expressing the level of turbulence in the flow, is well below the threshold required for turbulence (~2000 for flow in a channel) for all experiments. The Péclet number (Pe), which determines the dominance of advection versus conductive cooling, indicates that all flows examined are advection-dominated ($Pe >> 1$). Froude numbers for both the experiments and natural flows are less than one, highlighting that gravity is more significant than inertia for these flows. As discussed earlier, certain values of Ψ have been identified as marking transitions between flow morphologies. Calculations of Ψ are only relevant to our PEG and basalt experiments, since syrup experiments are isothermal. Our PEG experiments have Ψ values of ~2, appropriate for the rifted character of these experimental flows (Fig. 5). Natural flows in Hawai'i given in Table 1 have Ψ values appropriate for their channelized nature (32 for Mauna Loa 1984 and 118 for Kīlauea 1974). Controversially, using the same calculation, the calculated Ψ values for our basalt experiments are very large (> 2000), suggesting that the crust forms slowly relative to the advance of the flow. However, these flows are pillow-like and lobate in their appearance (Fig. 6). Details of the calculation are provided in the Supplementary Material.

Simple and compound lava flow fields

Lava flows span the space between two morphological end-members: *compound* flows and *simple* flows (Walker 1971). Compound flows are visibly divisible into multiple lobes and units, and simple flows are not. Walker (1971) interpreted these differences to reflect low effusion rates leading to compound flows, compared with that leading to simple flows. The majority of flows produced in our experiments had a single lobe or single channel morphology, and can therefore be considered simple flows. Many natural lava flows share this morphology, advancing within a central channel or as one main flow lobe with few breakouts and bifurcations. For such flows, the influence of substrate roughness will likely resemble that of our experiments; they will experience an initial significant reduction in flow velocity, followed by a diminishing influence of substrate roughness on velocity with time. However, other natural flows, particularly pāhoehoe flows with slow advance rates, such as those at Kīlauea, are emplaced through a complex sequence of advancing and inflating lobes initiated by the development of breakouts, eventually forming compound flow fields (e.g., Macdonald 1953; Swanson 1973; Hon et al. 1994). For such flows, each new breakout and every flow lobe will interact with local bed roughness as if it were a

new flow advancing from a primary source. As discussed in previous studies (e.g., Crisp and Baloga 1990; Hon et al. 1994; Hamilton et al. 2013), coarse pre-existing topography at the scale of a few centimeters impacts pāhoehoe flow lobes as they are first emplaced onto a new surface, prior to subsequent inflation. Our study confirms their field observations that advance of individual breakouts in a compound pāhoehoe flow is impeded or redirected by coarser substrates. The combined effects of decreased velocity and increased breakout number (because rougher substrates encourage breakout development, as apparent in Figs. 6 and 7) will act to slow the overall downslope advance rate and promote lateral expansion.

Implications for flow modeling

A key goal of our experiments was to assess how the influence of bed roughness can be introduced into lava flow emplacement models. One possibility is to incorporate the influence of the bed roughness into the effective viscosity of the lava, as both higher viscosity and rougher substrates act to slow the flows down. To do this, we examine an analytical expression for the advance of a viscous flow on sloping plane (Lister 1992):

$$X(t) = \left[(\rho g)^3 Q^4 \sin^5\alpha / 9\, \eta_{app}^3 \cos^2\alpha \right]^{1/9} t^{7/9} \qquad (1)$$

where X is the flow front position, t is time, ρ is the fluid density, g is gravitational acceleration, Q is the volumetric flux of material, α is the bed slope, and η_{app} is the liquid's apparent viscosity. Using a least square curve fitting technique, we calculated the apparent viscosity for each of the experiments. Results are given by the solid lines in Fig. 8. For PEG and basalt experiments, we performed this inversion only for the early part of the flow, before solidification became dominant. The fact that the flows of each material were all performed on the same slope and with very similar volumetric flux assisted in the isolation of apparent viscosity from other parameters that could have influenced the advance rate.

This procedure revealed that for corn syrup, the influence of the increase in GS from 0.012 to 1.0 cm (an increase in R from 0.03 to 2) was equivalent to a linear increase by a factor of 11.9 in η_{app}. For PEG, the same increase in GS (an increase in R from 0.014 to 1.0) resulted in an increase by a factor of 2.8 in η_{app}; however, for PEG, the relationship between GS and η_{app} was not linear. For molten basalt, it was difficult to evaluate the influence of bed roughness directly on effective viscosity, since not all runs had the same initial lava temperature (run 2 and run 3 "erupted" at $T > 1300\ °C$, while the others were at $T \sim 1250\ °C$). Nonetheless, for a given emplacement temperature, rougher substrate and larger grain sizes corresponded to a higher η_{app} for basalt as well.

Using the result from the corn syrup experiments, we propose that a "bed roughness" factor can be added to flow advance models via an increase in the effective lava viscosity. The factor may be linear, such as the case for corn syrup, or possibly more complex for different fluid rheologies (e.g., Bingham or Herschel-Bulkley fluids), and should thus be calibrated and evaluated for natural flows. A natural next step should be integration of a bed roughness quantity into thermo-mechanical flow emplacement models (e.g., FLOWGO, MAGFLOW, LavaSIM) where it will be folded into the effective lava viscosity. In parallel to future field and laboratory work, further advancement can be achieved through three-dimensional dynamic numerical models of flow emplacement, which will expand the parameter space available in the laboratory experiments and examine the influence of vertical versus lateral roughness variability, different material properties, and variable flux, flow thickness, and different velocities and thermal conditions. A systematic examination of the thermal and mechanical interactions at the lava–substrate boundary will provide a firm understanding of the temporal and geometric scales at which the effects of substrate roughness are important.

Current hazard assessments for lava flows in volcanic regions usually focus on predicting lava inundation areas and flow paths (e.g., Wadge et al. 1994; Rowland et al. 2005; Connor et al. 2012; Ganci et al. 2012; Herault et al. 2009). Yet an important aspect of hazard assessment is estimating advance rates and the time it will take an active lava flow to reach key facilities (e.g., Favalli et al. 2005; Solana et al. 2008; Harris and Rowland 2015). Our findings suggest that in order to improve estimates of flow advance rate, it will be advisable to prepare maps and digital models of bed roughness amplitude and spatial distribution in advance, before an eruption crisis is underway, and to routinely update these maps and digital data sets. This way, the roughness can be readily integrated into flow advance estimates when an eruption begins and as a crisis develops. As discussed earlier, new developments in remote sensing technology, including expanded satellite imagery coverage, airborne laser altimetry, and the increasing popularity of unmanned aerial systems, now allow scientists to quickly and inexpensively collect large amounts of data over areas of interest (e.g., Patrick et al. 2017; Turner et al. 2017; Favalli et al. 2018). These datasets can be harnessed to quantify bed roughness that can be integrated into flow prediction models in preparation for eruptions or implemented during an eruption. We envision a procedure similar to that taken in hydrology and oceanography, which utilized maps of the "Manning bed roughness index" (Limeranos et al. 1970) in flood and stream models (e.g., Horritt and Bates 2002; Candela et al. 2005; Kim et al. 2010).

Conclusions

Three sets of analog experiments (using corn syrup, PEG, and molten basalt) were performed to study the influence of substrate roughness on the advance rate and morphology of lava flows. For each set of experiments, flow advance rate and flow perimeter morphology were influenced by bed roughness. Substrates with larger grain sizes caused experimental flows to advance more slowly than finer substrates. Over time, as void spaces were filled and a thermal boundary layer developed, the reduction of velocity diminished. We discuss a simple formulation to incorporate the influence of bed roughness into flow advance models, acknowledging that this "roughness factor" needs to be calibrated for different volcanic environments and flow styles. Additionally, flow perimeters became more complex with emplacement on coarser substrates. This confirms field observations that topographic roughness on the order of 15% of flow thickness affects the path of active basaltic pāhoehoe flows. Based on our findings, we postulate that the inclusion of substrate properties in models used for lava hazard assessment and crisis response is likely to improve accuracy of predictions of flow paths and advance rates, thereby increasing the potential to save property, community infrastructure, and costs associated with lava flow inundation.

References

Behncke B, Neri M, Nagay A (2005) Lava flow hazard at Mount Etna (Italy): new data from a GIS-based study. Geol Soc Am Spec Pap 396:189–208

Blake S, Bruno BC (2000) Modelling the emplacement of compound lava flows. Earth Planet Sci Lett 184:181–197

Bridges NT (1992) Laboratory models of lava domes. M.S. Thesis, Arizona State University

Brown RJ, Thordarson T, Self S, Blake S (2015) Disruption of tephra fall deposits caused by lava flows during basaltic eruptions. Bull Volcanol 77:90. https://doi.org/10.1007/s00445-015-0974-3

Candela A, Noto LV, Aronica G (2005) Influence of surface roughness in hydrological response of semiarid catchments. J Hydrol 313(3–4): 119–131

Cappello A, Herault A, Bilotta G, Ganci G, Del Negro C (2015) MAGFLOW: a physics-based model for the dynamics of lava-flow emplacement. Geol Soc Lond 426:357–373. https://doi.org/10.1144/SP426.16

Carslaw HS, Jaeger JC (1959) Conduction of heat in solids, 2nd edn. Clarendon Press, Oxford

Cashman KV, Kerr RC, Griffiths RW (2006) A laboratory model of surface crust formation and disruption on lava flows through non-uniform channels. Bull Volcanol 68(7–8):753–770

Cashman KV, Soule SA, Mackey BH, Deligne NI, Deardorff ND, Dietterich HR (2013) How lava flows: new insights from applications of lidar technologies to lava flow studies. Geosphere 9(6): 1664–1680

Castruccio A, Rust A, Sparks RSJ (2010) Rheology and flow of crystal-bearing lavas: insights from analogue gravity currents. Earth Planet Sci Lett 297:471–480

Chevrel MO, Platz T, Hauber E, Baratoux D, Lavallée Y, Dingwell DB (2013) Lava flow rheology: a comparison of morphological and petrological methods. Earth Planet Sci Lett 384:109–120

Connor LJ, Connor CB, Meliksetian K, Savov I (2012) Probabilistic approach to modeling lava flow inundation: a lava flow hazard assessment for a nuclear facility in Armenia. J Appl Volcanol 1(1):3

Cordonnier B, Lev E, Garel F (2015) Benchmarking lava-flow models. Geol Soc Spec Publ 426:425–445. https://doi.org/10.1144/SP426.7

Crisp J, Baloga S (1990) A model for lava flows with two thermal components. J Geophys Res 95(82):1255–1270

Crown DA, Ramsey MS (2017) Morphologic and thermophysical characteristics of lava flows southwest of Arsia Mons, Mars. J Volcanol Geotherm Res 342(2017):13–28

Dietterich HR, Cashman KV (2014) Channel networks within lava flows: formation, evolution, and implications for flow behavior. J Geophys Res Earth Surf 119:1704–1724. https://doi.org/10.1002/2014JF003103

Dietterich HR, Cashman KV, Rust AC, Lev E (2015) Diverting lava flows in the lab. Nat Geosci 8:494–496. https://doi.org/10.1038/ngeo2470

Dietterich HR, Lev E, Chen J, Richardson JA, Cashman KV (2017) Benchmarking computational fluid dynamics models of lava flow simulation for hazard assessment, forecasting, and risk management. J Appl Volcanol 6:9. https://doi.org/10.1186/s13617-017-0061-x

Dragoni M (1989) A dynamical model of lava flows cooling by radiation. Bull Volcanol 51:88–95

Edwards BR, Karson J, Wysocki R, Lev E, Bindeman I, Kueppers U (2013) Insights on lava ice/snow interactions from large-scale basaltic melt experiments. Geology 41:851–854. https://doi.org/10.1130/G34305.1

Fagents SA, Greeley R (2001) Factors influencing lava-substrate heat transfer and implications for thermomechanical erosion. Bull Volcanol 62:519–532

Fagents SA, Rumpf ME, Crawford IA, Joy KH (2010) Preservation potential of implanted solar wind volatiles in lunar palaeoregolith deposits buried by lava flows. Icarus 207:595–604

Favalli M, Pareschi M, Neri A, Isola I (2005) Forecasting lava flow paths by a stochastic approach. Geophys Res Lett 32:L03305

Favalli M, Tarquini S, Fornaciai A (2011) DOWNFLOW code and LIDAR technology for lava flow analysis and hazard assessment at Mount Etna. Ann Geophys 54:5. https://doi.org/10.4401/ag-5339

Favalli M, Fornaciai A, Nannipieri L, Harris A, Calvari S, Lormand C (2018) UAV-based remote sensing surveys of lava flow fields: a case study from Etna's 1974 channel-fed lava flows. Bull Volcanol 80(3):29

Ferlito C, Siewert J (2006) Lava channel formation during the 2001 eruption on Mount Etna: evidence for mechanical erosion. Phys Rev Lett 96(2):028501. https://doi.org/10.1103/PhysRevLett.96.028501

Fink JH, Griffiths RW (1990) Radial spreading of viscous gravity currents with solidifying crust. J Fluid Mech 221:485–509

Fink JH, Griffiths RW (1992) A laboratory analog study of the surface morphology of lava flows extruded from point and line sources. J Volcanol Geothermal Res 54:19–32

Fink JH, Bridges NT, Grimm RE (1993) Shapes of Venusian "pancake" domes imply episodic emplacement and silicic composition. Geophys Res Lett 20(4):261–264

Fujita E, Hidaka M, Goto A, Umino S (2009) Simulations of measures to control lava flows. Bull Volcanol 71:401–408

Furbish DJ (1997) Fluid physics in geology: an introduction to fluid motions on Earth's surface and within its crust. Oxford University Press, Oxford

Ganci G, Vicari A, Cappello A, Del Negro C (2012) An emergent strategy for volcano hazard assessment: from thermal satellite monitoring to lava flow modeling. Remote Sens Environ 119:197–207

Giordano D, Russell JK, Dingwell DB (2008) Viscosity of magmatic liquids: a model. Earth Planet Sci Lett 271(1–4):123–134

Glaze LS, Baloga SM, Fagents SA, Wright R (2014) The influence of slope breaks on lava flow surface disruption. J Geophys Res Solid Earth 119:1837–1850. https://doi.org/10.1002/2013JB010696

Gregg TKP, Fink JH (1996) Quantification of extraterrestrial lava flow effusion rates through laboratory simulations. J Geophys Res 101(E7):16,891–16,900

Gregg TKP, Fink JH (2000) A laboratory investigation into the effects of slope on lava flow morphology. J Volcanol Geotherm Res 96:145–159

Gregg TK, Keszthelyi LP (2004) The emplacement of pahoehoe toes: field observations and comparison to laboratory simulations. Bull Volcanol 66:381–391

Griffiths RW (2000) The dynamics of lava flows. Annu Rev Fluid Mech 32(1):477–518

Griffiths RW, Fink JH (1992) The morphology of lava flows in planetary environments: predictions from analog experiments. J Geophys Res 97(19):739–748

Hamilton CW, Glaze LS, James MR, Baloga SM (2013) Topographic and stochastic influences on pāhoehoe lava lobe emplacement. Bull Volcanol 75(11):756

Harris AJL, Rowland SK (2001) FLOWGO: a kinematic thermo-rheological model for lava flowing in a channel. Bull Volcanol. 63:20–44 https://doi.org/10.1007/s004450000120

Harris AJL, Rowland SK (2009) Effusion rate controls on lava flow length and the role of heat loss: a review. Studies in volcanology: the legacy of George Walker. IAVCEI Spec Pub 2:33–51

Harris AJL, Rowland SK (2015) Flowgo 2012. In: Carey R, Cayol V, Poland M, Weis D (eds) Hawaiian Volcanoes. https://doi.org/10.1002/9781118872079

Harris AJL, Butterworth AL, Carlton RW, Downey I, Miller P, Navarro P, Rothery DA (1997) Low-cost volcano surveillance from space: case studies from Etna, Krafla, Cerro Negro, Fogo, Lascar and Erebus. Bull Volcanol 59:49–64

Harris AJL, Flynn LP, Keszthelyi L, Mouginis-Mark PJ, Rowland SK, Resing JA (1998) Calculation of lava effusion rates from Landsat TM data. Bull Volcanol 60:52–71

Herault A, Vicari A, Ciraudo A, Del Negro C (2009) Forecasting lava flow hazards during the 2006 Etna eruption: using the MAGFLOW cellular automata model. Comput Geosci 35(5):1050–1060

Herault A, Bilotta G, Vicari A, Rustico E, Del Negro C (2011) Numerical simulation of lava flow using a GPU SPH model. In: Del Negro C, Gresta S (eds) The lava flow invasion hazard map at Mount Etna and methods for its dynamic update. Annals Geophys. 54(5) https://doi.org/10.4401/ag-5343

Heslop SE, Wilson L, Pinkerton H, Head JW (1989) Dynamics of a confined lava flow on Kilauea volcano, Hawaii. Bull Volcanol 51:415–432

Hidaka M, Goto A, Umino S, Fujita E (2005) VTFS project: development of the lava flow simulation code LavaSIM with a model for three-dimensional convection, spreading, and solidification. Geochem Geophys Geosyst 6:Q07008. https://doi.org/10.1029/10.1029/2004GC000869

Hon K, Kauahikaua J, Denlinger R, McKay K (1994) Emplacement and inflation of pahoehoe sheet flows: observations and measurements of active lava flows on Kilauea volcano, Hawaii. Geol Soc Am Bull 106:351–370

Hoover SR, Cashman KV, Manga M (2001) The yield strength of subliquidus basalts—experimental results. J Volcanol Geotherm Res 107(1–3):1–18

Horritt MS, Bates PD (2002) Evaluation of 1D and 2D numerical models for predicting river flood inundation. J Hydrol 268(1):87–99

Kerr RC, Griffiths RW, Cashman KV (2006) Formation of channelized lava flows on an unconfined slope. J Geophys Res 111:B10206. https://doi.org/10.1029/2005JB004225

Keszthelyi L (1995) Measurements of the cooling at the base of pahoehoe flows. Geophy Res Lett 22(16):2195–2198

Keszthelyi L, Denlinger R (1996) The initial cooling of pahoehoe flow lobes. Bull Volcanol 58:5–18

Keszthelyi L, Self S (1998) Some physical requirements for the emplacement of long basaltic lava flows. J Geophys Res 103(ll):27447–27464

Keszthelyi L, Harris AJL, Dehn J (2003) Observations of the effect of wind on the cooling of active lava flows. Geophys Res Lett 30(19). https://doi.org/10.1029/2003GL017994

Kim JS, Lee CJ, Kim W, Kim YJ (2010) Roughness coefficient and its uncertainty in gravel-bed river. Water Sci Eng 3:2

Kundu PK, Cohen IM (2004) Fluid mechanics, 3rd edn. Academic Press, Cambridge

Limerinos JT, California. Dept. of Water Resources (1970) Determination of the Manning coefficient from measured bed roughness in natural channels. USGS Water Suppl Pap 1898-B

Lu Z, Masterlark T, Dzurisin D (2005) Interferometric synthetic aperture radar study of Okmok volcano, Alaska, 1992–2003: magma supply dynamics and postemplacement lava flow deformation. J Geophys Res Solid Earth, 110(B2)

Macdonald GA (1953) Pahoehoe, aa, and block lava. Am J Sci 251:169–191

Moore HJ (1987) Preliminary estimates of the rheological properties of 1984 Mauna Loa lava. US Geol Surv Prof Pap 1350:1569–1588

Müller D, Walter TR, Schöpa A, Witt T, Steinke B, Gudmundsson MT, Dürig T (2017) High-resolution digital elevation modeling from TLS and UAV campaign reveals structural complexity at the 2014/2015 Holuhraun eruption site, Iceland. Front Earth Sci 5:59

Oppenheimer C (1991) Lava flow cooling estimated from Landsat thematic mapper infrared data: the Lonquimay eruption (Chile, 1989). J Geophys Res 96:21,865–21,878

Patrick MR, Dehn J, Dean K (2004) Numerical modeling of lava flow cooling applied to the 1997 Okmok eruption: approach and analysis. J Geophys Res 109:B03202. https://doi.org/10.1029/2003JB002537.

Patrick M, Orr T, Fisher G, Trusdell F, Kauahikaua J (2017) Thermal mapping of a pāhoehoe lava flow, Kīlauea Volcano. J Volcanol Geotherm Res 332:71–87

Pinkerton H, Sparks RSJ (1978) Field measurements of the rheology of lava. Nature 276(5686):383–385

Pinkerton H, Wilson L (1994) Factors controlling the lengths of channel fed lava flows. Bull Volcanol 56:108–120

Proietti C, Coltelli M, Marsella M, Fujita E (2009) A quantitative approach for evaluating lava flow simulation reliability: LavaSIM code applied to the 2001 Etna eruption. Geochem Geophys Geosyst 10:Q09003. https://doi.org/10.1029/2009GC002426

Richter N, Favalli M, de Zeeuw-van Dalfsen E, Fornaciai A, da Silva Fernandes RM, Rodriguez NP, Levy J, Victória SS, Walter TR (2016) Lava flow hazard at Fogo Volcano, Cape Verde, before and after the 2014–2015 eruption. Nat Hazards Earth Syst Sci Discuss. https://doi.org/10.5194/nhess-2016-81

Rowland SK, Walker GPL (1990) Pahoehoe and aa in Hawaii: volumetric flow rate controls the lava structure. Bull Volcanol 52:615–628. https://doi.org/10.1007/BF00301212

Rowland S, Garbeil H, Harris A (2005) Lengths and hazards from channel-fed lava flows on Mauna Loa, Hawai'i, determined from

thermal and downslope modeling with FLOWGO. Bull Volcanol 67:634–647

Rumpf ME, Fagents SA, Crawford IA, Joy KH (2013a) Numerical modeling of lava-regolith heat transfer on the moon and implications for the preservation of implanted volatiles. J Geophys Res Planet 118:382–397. https://doi.org/10.1029/2012JE004131

Rumpf ME, Fagents SA, Hamilton CW, Crawford IA (2013b) Numerical and experimental approaches toward understanding lava flow heat transfer, Eos Trans. AGU, Fall Mtg. Suppl., Section Abs. V51D-2707

Scifoni S, Coltelli M, Marsella M, Proietti C, Napoleoni Q, Vicari A, Del Negro C (2010) Mitigation of lava flow invasion hazard through optimized barrier configuration aided by numerical simulation: the case of the 2001 Etna eruption. J Volcanol Geotherm Res 192(1–2):16–26

Scott WE (1989) Volcanic hazard zonation and long-term forecasts, In Volcanic hazards, Short Courses in Geol, V1, ed. RI Tilling, AGU, 25–49

Siewert J, Ferlito C (2008) Mechanical erosion by flowing lava. Contempor Phys 49(1):43–54. https://doi.org/10.1080/00107510802077388

Solana MC, Kilburn CRJ, Rolandi G (2008) Communicating eruption and hazard forecasts on Vesuvius, southern Italy. J Volcanol Geotherm Res 172(3–4):308–314

Soule SA, Cashman KV (2005) The shear rate dependence of the pahoehoe-to-aa transition: analog experiments. Geology 33:361–364

Stasiuk MV, Jaupart C, Stephen R, Sparks J (1993) Influence of cooling on lava-flow dynamics. Geology 21(4):335–338

Swanson D (1973) Pahoehoe flows from the 1969-1971 Mauna Ulu eruption, Kilauea volcano, Hawaii. Geol Soc Am Bull 84:615–626

Tarolli (2014) High-resolution topography for understanding Earth surface processes: opportunities and challenges. Geomorph 216:295–312

Tarquini S (2017) A review of mass and energy flow through a lava flow system: insights provided from a non-equilibrium perspective. Bull Volcanol 79(8):64

Tarquini S, Favalli M (2011) Mapping and DOWNFLOW simulation of recent lava flow fields at Mount Etna. J Volcanol and Geotherm Res 204:27–39

Turner NR, Perroy RL, Hon K (2017) Lava flow hazard prediction and monitoring with UAS: a case study from the 2014–2015 Pāhoa lava flow crisis, Hawai'i. J Appl Volcanol 6(1):17

Wadge G, Young PAV, McKendrick IJ (1994) Mapping lava flow hazards using computer simulation. J Geophysic Res Solid Earth 99(B1): 489–504

Walker GPL (1967) Thickness and viscosity of Etnean lavas. Nature 213: 484–485

Walker GPL (1971) Compound and simple lava flows and flood basalts. Bull Volcanol 35:579–590

Walker GPL (1973) Lengths of lava flows, in guest, JE, and Skelhorn, RR, eds., Mount Etna and the 1971 eruption. Philosoph Trans R Soc London A 274(1238):107–118

Whelley PL, Glaze LS, Calder ES, Harding DJ (2014) LiDAR-derived surface roughness mapping: applications to Mount St. Helens Pumice Plain deposit analysis. IEEE Trans Geosci Remote Sens 52(1):426–438. https://doi.org/10.1109/TGRS.2013.2241443

Wolovick MJ, Creyts TT, Buck WR, Bell RE (2014) Traveling slippery patches produce thickness-scale folds in ice sheets. Geophys Res Lett 41(24):8895–8901

Lister JR (1992) Viscous flows down an inclined plane from point and line sources. J Fluid Mech 242:631–653